Construction and Building Materials 369 (2023) 130512

Contents lists available at ScienceDirect

Construction and Building Materials

journal homepage: www.elsevier.com/locate/conbuildmat

Cyclic heat-generation and storage capabilities of self-heating cementitious composite with an addition of phase change material

Daeik Jang [a], H.N. Yoon [a], Beomjoo Yang [b], Hammad R. Khalid [c,d,*]

[a] Department of Civil and Environmental Engineering, Korea Advanced Institute of Science and Technology (KAIST), 291 Daehak-ro, Yuseong-gu, Daejeon 34141, Republic of Korea
[b] School of Civil Engineering, Chungbuk National University, 1 Chungdae-ro, Seowon-gu, Cheongju, Chungbuk 28644, Republic of Korea
[c] Civil and Environmental Engineering Department, King Fahd University of Petroleum and Minerals (KFUPM), Dhahran 31261, Saudi Arabia
[d] Interdisciplinary Research Center for Construction and Building Materials, King Fahd University of Petroleum and Minerals (KFUPM), Dhahran 31261, Saudi Arabia

ARTICLE INFO

Keywords:
Phase change material
Latent heat
Self-heating
Heat storage capacity
Cement composite

ABSTRACT

This study explored the efficiency of the phase-change materials (PCM) to improve the heat storage capacity of carbon nanotube (CNT) and carbon fiber (CF) based self-heating cementitious composites. Composites were prepared with 0.8 wt% CNT and 0.2 wt% CF as conductive fillers, and five different PCM contents (0, 5, 10, 20, and 30 wt%), and their electrical conductivities, thermal conductivities, and compressive strengths were measured. To determine the self-heating capability, the heat-generation and heat-storage capabilities of the composites were investigated using monotonic and cyclic heating/cooling tests. The results of these tests were analyzed through a differential scanning calorimetry and micro-computed tomography, which showed that the PCM particles with high latent heat were well dispersed in the composites, improving the heat storage capacity. Therefore, it can be said that the addition of PCM may improve heat storage capacity and enhance energy efficiency of the cement-based self-heating composites.

1. Introduction

Conductive cementitious composites are attracting increasing attention as they have a wide range of applications including piezoresistive sensors for structural health monitoring [1–5], electromagnetic interference shielding composites [6–9], and self-heating composites [10–13]. Early research on conductive cementitious composites used conventional conductive fillers, such as carbon-based (e.g., carbon black and graphite) and steel-based (e.g., steel fiber and iron powder) fillers, to achieve favorable electrical conductivity [14–17]. However, large amounts of these fillers (i.e., greater than 5 wt%) are required to produce conductive cementitious composites with favorable electrical conductivity [18,19]. In addition, corrosion can occur when steel-based fillers are used, which dramatically reduces the electrical conductivity. Accordingly, many researchers have investigated multi-walled carbon nanotubes (CNTs) for use as conductive fillers in cementitious composites, as they have excellent mechanical, electrical, and thermal properties [20–22]. Furthermore, several studies have considered the synergistic effects of different combinations of conductive fillers to mitigate their individual limitations. For example, Kim et al. [23] reported that a combination of CNTs and carbon fiber (CF) can improve the electrical and thermal characteristics of conductive cementitious composites, and can enhance their heat generation capability for use in self-heating systems. Moreover, Yoon et al. [24] reported that this combination had a positive synergistic effect on the electrical conductivity and electromagnetic wave shielding capability, and found notable improvements in both electrical conductivity and functional capability.

Many studies have explored the application of conductive cementitious composites as self-heating composites [25–29]. The fillers produce conductive pathways in the composites, and, heat is produced as current flows through them via the Joule's heating mechanism [30]. Liu et al. [31] fabricated cementitious composites embedded with carbon nanofiber, which provided insights into self-heating composites for the construction in cold regions. Kim et al. [25] and Choi et al. [32] examined the self-heating capability of CNT/cement composites under cyclic heating conditions. Authors reported that the electrical instability occurred during heating cycles, which can affect the stable heat generation during their service life. Jang et al. [33] used silica aerogel to

* Corresponding author at: Civil and Environmental Engineering Department, King Fahd University of Petroleum and Minerals (KFUPM), Dhahran 31261, Saudi Arabia.
E-mail address: hammad.khalid@kfupm.edu.sa (H.R. Khalid).

https://doi.org/10.1016/j.conbuildmat.2023.130512
Received 2 August 2022; Received in revised form 12 January 2023; Accepted 23 January 2023
Available online 3 February 2023

mitigate the disturbance of CNT-based conductive networks, and demonstrated composites with improved self-heating capability during cyclic heating.

Many researchers have focused on methods to improve the electrical and heating stabilities of cement-based heating composites. In contrast, little effort has been made to examine their heat-storage performance, which is an important factor in the development of self-heating systems [30]. Recently, researchers have begun to use PCMs to improve the heat storage capacity of cementitious composites. For example, Frąc et al. [34] incorporated paraffin, a type of PCM, into cementitious composites for heat storage and demonstrated its potential to improve the heat storage capacity. In addition, Kim et al. [35] reported that the addition of a PCM-impregnated aggregate can enhance the thermal stability and durability owing to the latent heat properties of the PCM during the heating and free cooling processes. However, comprehensive studies on the stability of the self-heating performance and heat storage capacity of cement-based self-heating composites in cyclic heating/cooling environments were not actively taken into consideration up to date.

Thus, this study aims to investigate the effects of PCMs on the self-heating performance and heat storage capacity of cement-based self-heating composites. The composites were prepared with conductive fillers including both MWCNT 0.8 wt% and CF 0.2 wt% due to their synergistic effects on improvements of electrical conductivity [24]. Four different PCM contents (0, 5, 10, 20, and 30 wt%) were additionally added to the composites, and their compressive strengths, and electrical and thermal conductivities were characterized. In addition, their self-heating performance and heat storage capacity in cyclic heating and cooling environments were investigated, and the experimental results are discussed in terms of microstructural analyses, including differential scanning calorimetry (DSC) and micro-computed tomography (CT) observations.

2. Experimental procedure

2.1. Materials and sample preparation

Ordinary Portland cement (OPC) was used as the binder, and commercial multi-walled CNTs produced by thermal chemical vapor deposition (CVD; Jeio, Inc.) and polyacrylonitrile (PAN)-type CF (Ace C & Tech Co., ltd.) were used as conductive fillers. The CNTs and CF had diameters of approximately 10 nm and 7.2μ m and lengths of 100–200μ m and 3 mm, respectively. 10 % of silica fume (Elkem Inc., EMS-970) and 2 % of polycarboxylate-type superplasticizer (Dongnam Co., ltd., FLOWMIX 3000 L) by cement mass were added to improve the dispersion of the CNT agglomerates in the composites. The SiO_2 composition in the silica fume was greater than 95 %, and it had a particle diameter of approximately 5 μm. A commercial spherical-shaped capsulized paraffin-based PCM (Insilico Co. ltd.) was also added to the composites. The average capsule diameter and phase-change temperature of PCM were approximately 6μ m and 55 °C, respectively. Total five types of samples according to the PCM contents (0, 5, 10, 20, 30 wt%) were fabricated as summarized in Table 1. The conductive fillers including MWCNT 0.8 wt% and CF 0.2 wt% were added to form the conductive networks in the cement matrix.

Various methods of dispersing CNTs in cementitious composites have been reported in studies using CNTs in the cementitious composites [36–38]. These methods can be divided into two main types based on the use of ultrasonic treatment i.e., with and without ultrasonic treatment [36–39]. During ultrasonic treatment, ultrasonic waves interact with the CNT particles and reduce the effect of van der Waals forces, thereby improving dispersion [36–38]. However, this method requires additional experimental equipment, time, and cost, and may introduce unwanted air bubbles, which can decrease the mechanical strength of the composites [36–38]. Therefore, this study used a direct mechanical mixing without ultrasonic treatment to mitigate these issues. Furthermore, silica fume was used to infiltrate between the CNT particles, which increases the distance between them owing to the ball bearing effect [40]. A polycarboxylate-type superplasticizer, which can cause steric repulsion, was also used to reduce the van der Waals forces on the CNT particles and improve dispersion [40]. Furthermore, the different water-to-cement ratio was chosen to obtain the target flow (120 ± 10 mm), which is considered as the optimized flow value for dispersing CNTs in cementitious composites [33].

The samples were prepared as follows. The raw materials including cement, silica fume, CNTs, CF, and PCM were added to a Hobart mixer and mixed for 5 min at low speed. The solution (water and superplasticizer) was then poured into the mixture and mixed for 5 min at low speed, followed by an additional mixing for 3 min at high speed. The mixtures were poured into cubical molds with 50 mm sides, in accordance with previous studies [24,41,42]. Copper electrodes (70 mm long, 20 mm wide, and 0.3 mm thick) were prepared. They were painted with silver paste to minimize contact resistance between the composites and electrodes, and to protect the electrodes against corrosion. The prepared electrodes were embedded in the cubical molds with an embedment depth of 50 mm and a separation of 30 mm. Subsequently, the molds were wrapped by plastic tape to prevent unwanted moisture evaporation and natural carbonation, then cured in an oven at 25 °C. The samples were demolded after 1 day, then cured for an additional 27 days in the same oven.

2.2. Experimental details

The electrical characteristics and thermal conductivity of the samples were measured before their self-heating and heat storage capabilities were investigated. A digital multimeter (DMM 34410A) with the two-probe method was used to measure the electrical resistance, and the thermal conductivity was measured (TPS 2500 S Hot Disk AB device) based on ISO standard 22007–2 [41]. The compressive strength was measured using a compression testing machine (INSTRON). In every test, three replicates of each sample were used and the average values were calculated.

Two different heating tests (i.e., Monotonic and cyclic tests) were conducted to investigate the heat generation capability and heating stability, respectively. In the monotonic self-heating test, three different voltages (3, 5, and 8 V) were applied to the samples for 1 h using a DC power supply (PL-3005S). In the cyclic heating test, an identical input power of 10 W was applied for 30 min. During each heating test, the surface temperature and electrical current flowing through the samples were measured using a K-type thermocouple and data logger (Agilent Technologies 34972A), respectively. To investigate the heat storage

Table 1
Mix proportions of the samples (wt.%).

Sample Code	Cement	Silica fume	MWCNT	CF	PCM	Water	SP	w/c ratio	Target Flow (mm)
P0	100	10	0.8	0.2	0	36	2	0.36	120 ± 10
P5	100	10	0.8	0.2	5	37	2	0.37	
P10	100	10	0.8	0.2	10	38	2	0.38	
P20	100	10	0.8	0.2	20	43	2	0.43	
P30	100	10	0.8	0.2	30	47	2	0.47	

performance, the change in the surface temperature of the samples between 60 and 35 °C was measured in a cooling test. The time interval between 50 and 45 °C, where the PCM phase change occurred, was systematically investigated. The heating and cooling processes were repeated for 20 cycles to investigate the stability of the self-heating and heat storage performances of the samples. Furthermore, cyclic heating for 3 h and cooling for 2 h was repeated for five cycles, where an input power of 10 W was applied to the samples during every cycle. A zeta potential analyzer (ELSZ-2000, Otsukael) was chosen to measure the potential difference of the MWCNT and PCM as immersed in water, in order to observe the dispersion state of the CNT and PCM particles in the composites. A DSC analysis was performed using the measurement device (DSC1, Mettler Tolledo) to examine the latent heat and melting temperature of the PCM in the temperature range of 0–70 °C at a heating rate of 10 °C/min. Micro-CT (SkyScan 1172, Bruker) with a 100 kV X-ray was used for investigating the internal structures and PCM distribution in samples. Through, the micro-CT analysis, the volume percentage of PCM can be calculated which is related to the improvements of heat-storage capability.

3. Characterization of the samples

3.1. Electrical resistivity

The electrical resistivities of the samples are shown in Fig. 1. The electrical resistance was converted to electrical resistivity based on the area of the embedded electrodes and the distance between them i.e., 10 cm^2 and 3 cm, respectively [43]. In Fig. 1 (a), the effect of the PCM content on the electrical resistivity can be observed. As the PCM content increased, the electrical resistivity generally increased except the P5 sample. For P5 sample, it can be deduced that the PCM particle can be located between the CNT particles, increasing the distance of the adjacent CNT particles. Thus, it can increase the dispersion state and decrease the electrical resistivity. Except the P5 sample, similar results have been reported in previous studies, which showed that the addition of nonconductive fillers into CNT-based composites can increase the overall electrical resistivity [30,33]. Nonconductive fillers can hinder the formation of conductive networks by increasing the distance between adjacent CNT particles; thus, an excessive amount of PCM (i.e., 30 wt%) increased the electrical resistivity from 11.23 to 70.47 Ω-cm (Fig. 1 (a)). However, it should be noted that all the samples, regardless of the PCM content, showed much lower electrical resistivity (i.e., less than 100 Ω-cm) than those in similar studies, which reported that such electrical resistivity is favorable for use as self-heating composites [25,27,33]. It can be deduced that this is a result of synergy between the CNTs and CF, which can form hierarchical conductive pathways that reduce the effect of the nonconductive filler (i.e., PCM) on the overall electrical resistivity [23,44]. Therefore, the authors believe that all fabricated samples secured favorable electrical resistivity for use as self-heating composites (discussed in the experimental outcomes provided in the later sections of 4.2 and 4.3).

3.2. Thermal conductivity

The thermal conductivities of the samples, shown in Fig. 1 (b), decreased as the PCM content increased. Sample P0, which contained no

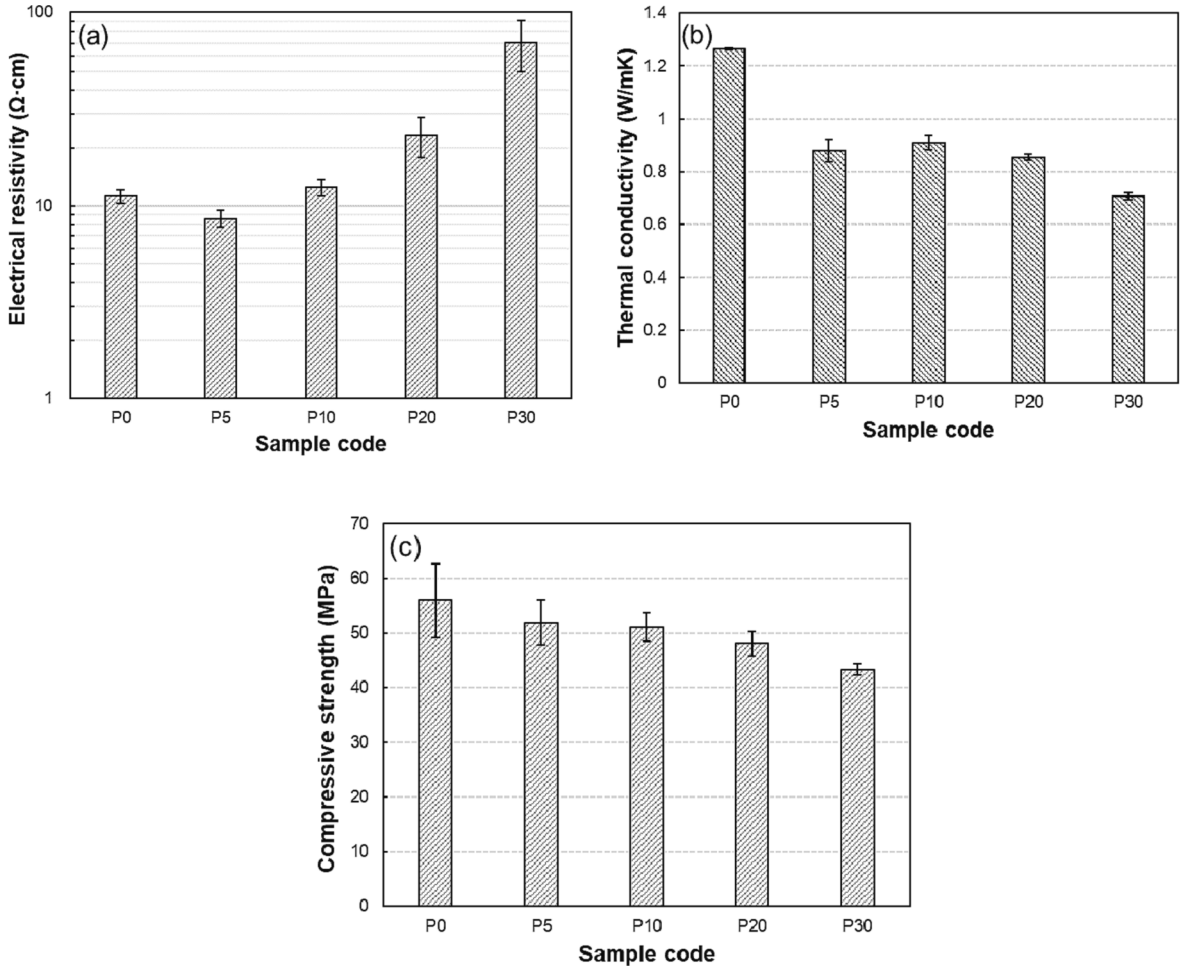

Fig. 1. (a) Electrical resistivity, (b) thermal conductivity, and (c) compressive strength of the samples.

PCM, showed thermal conductivity of 1.26 W/m-K. Then, the thermal conductivity tended to be decreased to 0.88, 0.91, 0.85, 0.71 W/m-K when PCM content was increased to 5, 10, 20, and 30 wt%, respectively. This represents reductions in thermal conductivity by 30.3 %, 28.1 %, 32.4 %, and 44.1 % compared to sample P0. There are two main factors that could explain this result, the PCM content and the water-to-cement ratio. First, the addition of a PCM with low thermal conductivity can reduce the overall thermal conductivity of the samples. Second, an increase in the water-to-cement ratio can also reduce the thermal conductivity. As summarized in Table 1, water-to-cement ratios of 0.36, 0.37, 0.38, 0.43, and 0.47 were used to fabricate samples P0, P5, P10, P20, and P30, respectively. It is known that a high water-to-cement-ratio can cause high porosity in cementitious composites, and the thermal conductivity decreases as the porosity increases owing to the super-low thermal conductivity of the air in the voids [45]. The thermal conductivity of the samples decreased as the PCM content increased, indicating its potential to increase the heat storage capacity which is discussed in *Sec*. 4. Interestingly, the P5 sample showed marginally lower thermal conductivity than that found in P10 sample. This small discrepancy in thermal conductivity values can also be attributed to marginal improvement in conductive network of this sample at a lower PCM content. The coupling effect of ternary fillers and the interfacial resistance between the fillers can also be the reasons for this behavior [46,47]. However, it should be noted that thermal conductivity of P5 sample is still similar to P10 sample considering the range of errors as shown in Fig. 1.

3.3. Compressive strength

The compressive strengths of the samples with different PCM contents are shown in Fig. 1 (c). The compressive strength of sample P0 was approximately 56 MPa. The compressive strength decreased to 52, 51, 48, and 43 MPa as the PCM content increased to 5, 10, 20 and 30 wt%, respectively. Overall, the compressive strength tended to decrease as the PCM content increased. The reduction in the compressive strength was probably caused by a combination of factors. First, the inclusion of PCM could weaken the bonds between PCM particles and the cement matrix, reducing the compressive strength [48]. Second, a high water-to-cement ratio could increase the porosity of the composites, reducing their compressive strength [20]. Nevertheless, all the samples, regardless of the PCM content, exhibited compressive strengths greater than 40 MPa.

4. Self-heating performance and heat-storage capacity of the samples

4.1. Electrical stability

The electrical stability of the samples is illustrated in Fig. 2, which shows the relationship between the input voltage and current. According to this relationship, the tunneling-induced electrical resistivity can be examined. The tunneling effect indicates that electrons in the CNT-embedded composites can probabilistically skip insulated layers between adjacent CNT particles, thereby reducing the electrical resistivity [49]. The relationship between the input voltage and current is shown in Fig. 2 (a), and the electrical resistances, obtained using Ohm's law and converted to electrical resistivity using the dimensions of the electrodes (70 mm length and 20 mm width), are shown in Fig. 2 (b) [50]. Fig. 2 (a) shows that the linearity, expressed as R^2, was approximately 0.99 when the input voltage was in the range 1–10 V, which indicates good electrical stability. However, it can be also seen that the electrical resistivity decreased to a greater extent in sample P30, compared to the other samples. This can be explained by the electrostatic interaction, expressed as the zeta potential, between the CNT and PCM particles. As summarized in Table 2, the CNT and PCM particles produced zeta potentials of −11.75 and −29.74 mV, respectively, when they were dispersed in water, which has a zeta potential of −16.9 mV. These values were converted to relative values, which showed that the CNT and PCM particles were positively (5.15 mV) and negatively (-12.84 mV) charged, respectively. These opposing charges indicate that CNT and PCM particles can attract each other through electrostatic interactions [30]. Thus, individual CNTs can attach to the incorporated-PCM, thereby increasing the distance between adjacent CNT particles. Consequently, a larger tunneling effect was observed in the samples with higher PCM content (i.e., P30), which is in good agreement with other related studies [30,51,52]. According to the tunneling-induced electrical resistivity as shown in Fig. 2, it can be inferred that the fabricated samples showed excellent electrical stability in the input voltage range 1–10 V, regardless of their PCM content.

4.2. Monotonic self-heating capacity

The self-heating performances of the samples, expressed as

Table 2
Zeta potentials values of the used MWCNT and PCM.

Sample	Water	MWCNT in water	PCM in water
Absolute value (mV)	−16.9	−11.75	−29.74
Relative value (mV)	0	5.15	−12.84

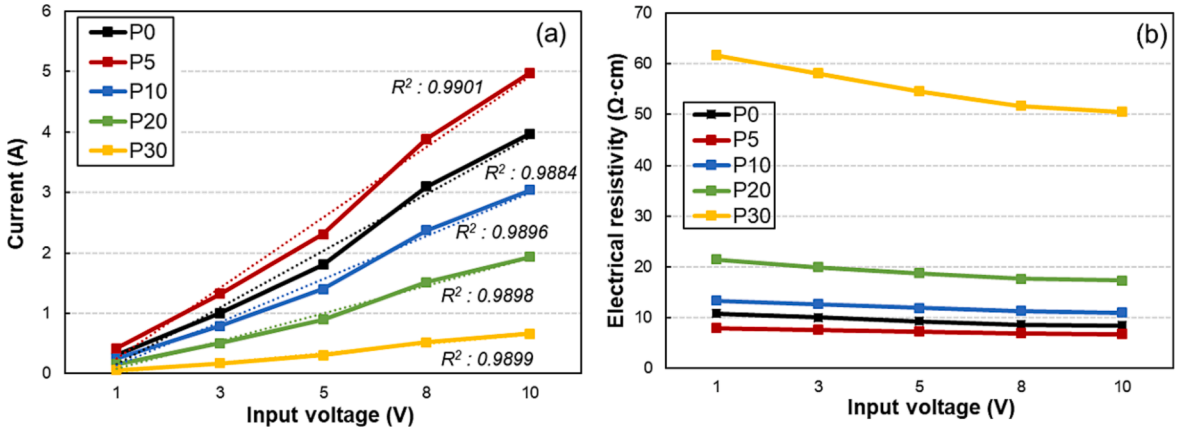

Fig. 2. Relationship between input voltage and (a) the current, and (b) the electrical resistivity of the samples.

temperature increases, are shown in Fig. 3. Based on the experimental results for electrical stability, shown in Fig. 2, input voltages of less than 10 V (i.e., 3, 5, and 8 V) were applied to the samples. Fig. 2 (a–c) shows that the samples were heated continuously for 1 h during the monotonic heating process. Thus, the surface temperature, shown in Fig. 3 (d), was different from the maximum temperature the samples could be heated to. Nonetheless, the surface temperature after 1 h of heating can be used to compare the self-heating performance under short-term heating conditions, and it has been considered as an important factor in previous studies [25,32,33]. From Fig. 3, samples P5 and P10, which had low PCM contents (i.e., 5 and 10 wt%), were heated to approximately 40, 60, and 90 °C, when input voltages of 3, 5, and 8 V were applied, respectively. These temperatures are similar to those recorded for sample P0, with no PCM. This can be deduced from the electrical resistivity shown in Fig. 1 (a) and Fig. 2 (b). The addition of 5–10 wt% of PCM did not significantly affect the electrical resistivity of the samples, and electrical resistivities of P5 and P10 were similar to that of P0 (Fig. 2).

Since the self-heating performance is determined by the electrical resistivity, the self-heating performances of samples P5 and P10 showed similar trends to that of P0. Moreover, comparable reductions in the self-heating performances were observed in samples P20 and P30, where an excessive amount of PCM was added. The micro-sized PCM particles can be attached to individual nano-size CNTs, which increases the distance between adjacent CNTs, thereby increasing the electrical resistivity. Hence, samples with high PCM contents were heated to much lower temperatures than samples P0, P5, and P10. Specifically, sample P30 had surface temperatures of approximately 30, 35, and 40 °C at input voltages of 3, 5, and 8 V, respectively. According to the monotonic self-heating test, it can be concluded that a higher input voltage is required to heat samples P20 and P30 than samples P0, P5, and P10.

4.3. Cyclic heat-generation performance

The self-heating performances of the samples under cyclic heating are shown in Fig. 4. In the monotonic heating test, different input voltages were required to heat the samples to similar temperatures.

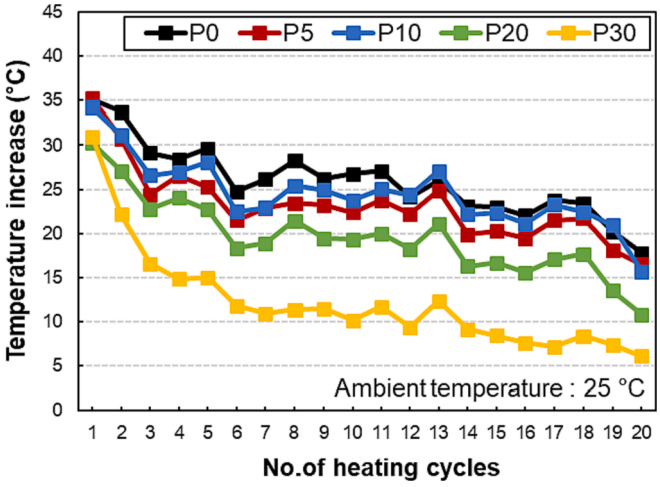

Fig. 4. Variations in the temperature increase of the samples observed in the cyclic heating.

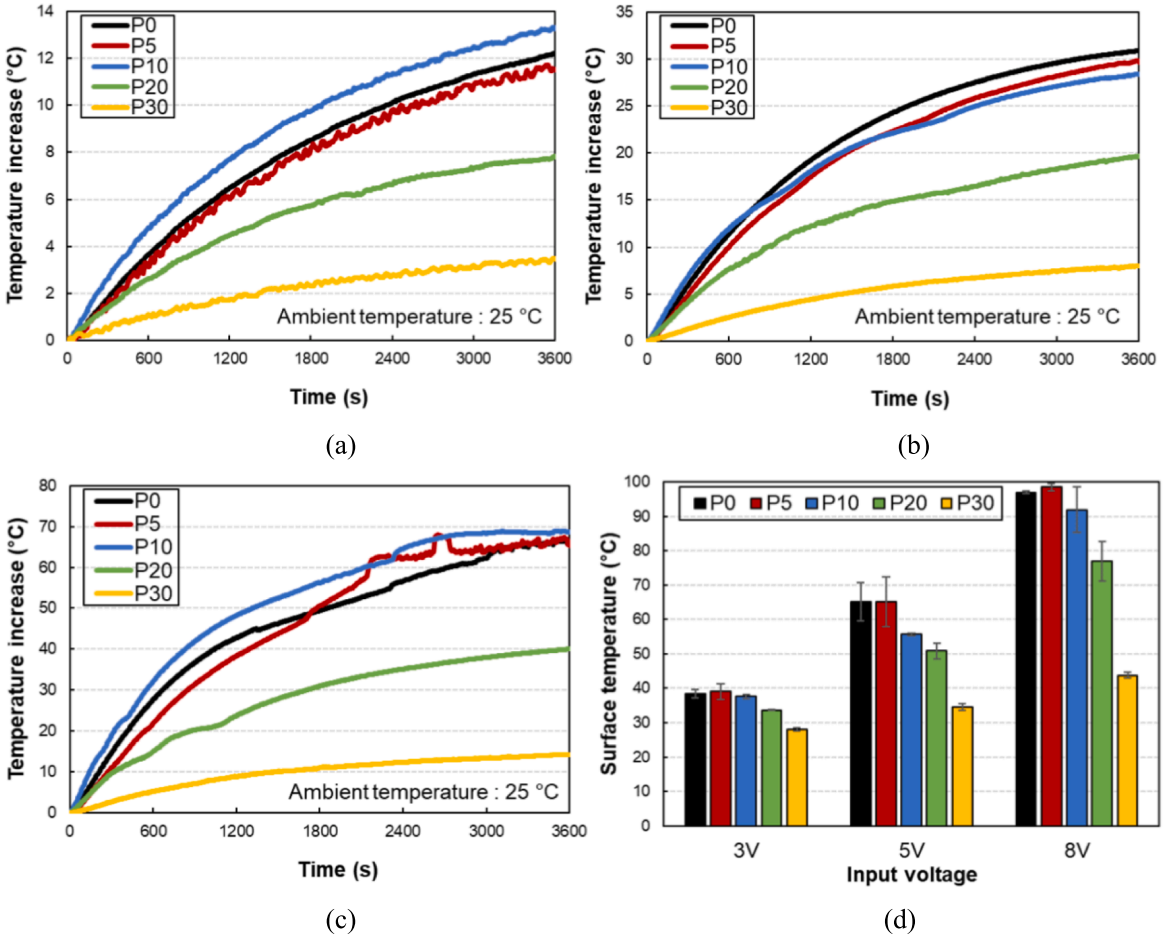

Fig. 3. Temperature increase when heated for 1 h with an input voltage of (a) 3 V, (b) 5 V, and (c) 8 V, and the maximum surface temperature of the samples.

Thus, in the cyclic heating test, an input power of 10 W was applied to the samples to achieve a favorable surface temperature (i.e., 60 °C) at 1st cycle. From 2nd cycle to 20th cycle, the same input voltage with 1st cycle is applied to the samples. As shown in Fig. 4, the temperature of the samples increased by approximately 35 °C which can be heated up to 60 °C. This similarity in the temperature increase of the samples can be

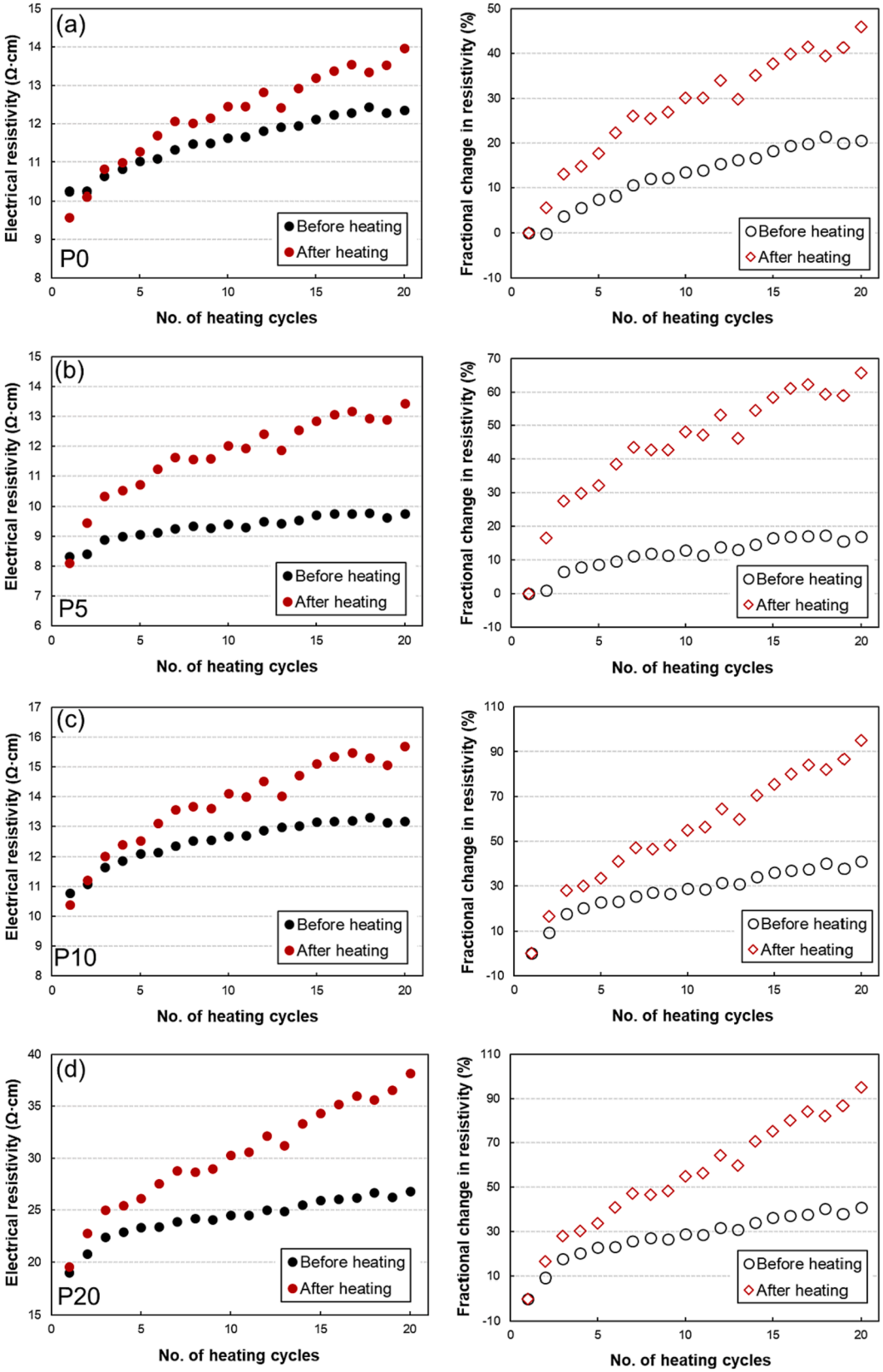

Fig. 5. Electrical resistivity (left) and fractional change in resistivity (right) of the (a) P0, (b) P5, (c) P10, (d) P20, and (e) P30 samples observed in the cyclic heating test.

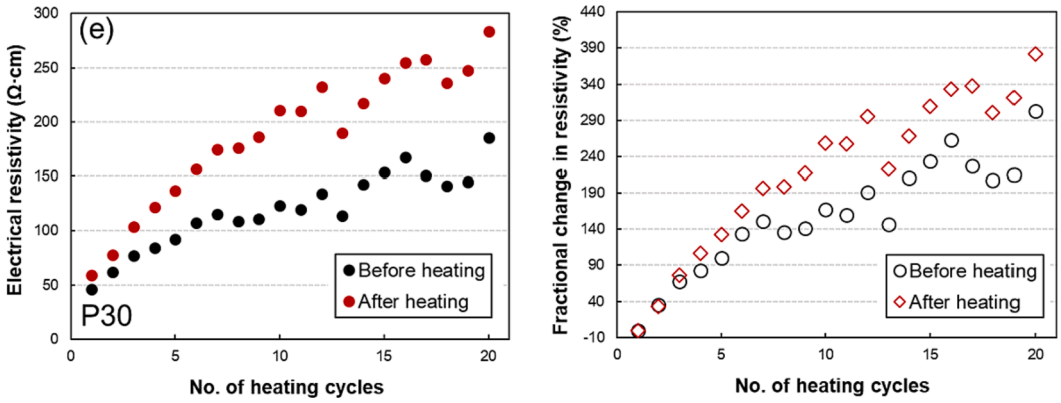

Fig. 5. (*continued*).

explained by Joule's heating law [33]. In addition, the maximum temperature increase of all the samples, regardless of the PCM content, decreased as the number of heating cycles increased. They all showed a temperature increase of approximately 35 °C during the first heating cycle, but this temperature increase dropped to increases of 17.8, 16.5, 15.7, 10.8, and 6.1 °C in samples P0, P5, P10, P20, and P30, respectively.

The heating capability was significantly affected by the electrical resistivity of the samples; thus, the electrical resistivity before and after heating for 30 min is shown in Fig. 5. The electrical resistivity measured before heating increased continuously during cyclic heating. This can be attributed to the additional hydration of the samples and the evaporation of residual moisture. When additional hydration occurs, the hydrates can hinder the movement of electrons flowing through the CNT-based conductive networks, thereby increasing the electrical resistivity [33]. In addition, internal void, which is caused by the evaporation of residual moisture, could also increase the electrical resistivity [33]. Therefore, the heating capability of the samples degraded, regardless of their PCM content, as shown in Fig. 4.

However, the extent of the reduction in temperature increase varied according to the PCM content, which can be seen at the 20th heating cycle in Fig. 4. According to previous studies, degradation of the heating capability is caused by the disturbance and redistribution of conductive networks during the heating process [25,33,53]. As shown in Fig. 5, to examine these disturbances and redistribution, the variation in electrical resistivity before and after heating was investigated. The electrical resistivity after heating was larger than that before heating. This can be explained by the positive temperature coefficient (PTC) effect, which indicates that the electrical resistivity of the composites increased as the temperature increased [54]. This effect occurs due to the expansion of the cement matrix as the temperature increases, which increases the distance between adjacent CNT and CF particles. This PTC effect occurred in all of the samples, but the fractional changes in electrical resistivity before and after heating differed according to the PCM content.

The PTC effect occurred during the heating process, and afterward the cement matrix and conductive fillers returned to their original positions as the temperature decreased. However, the PCM particles can hinder the conductive fillers as they return to their original positions. Therefore, the connectivity of the conductive fillers may be lower after cooling. The samples with higher PCM contents showed much larger increases in electrical resistivity. For examples, sample P0 showed a difference in electrical resistivity (1.62 Ω-cm) before and after heating, whereas samples P5, P10, P20, and P30 showed differences of 3.69, 2.52, 11.33, and 98.22 Ω-cm, respectively at 20th cycle. Based on the self-heating performance and the electrical stability during cyclic heating, it can be concluded that excessive PCM content can reduce the connectivity of conductive fillers during the disturbance and redistribution process.

4.4. Cyclic heat-storage capacity

The variation in the surface temperature of the samples was observed under the cyclic cooling test, as shown in Fig. 6. As described in *Sec.* 2, the phase-change temperature of the PCM was approximately 55 °C, whereas the temperature observed in Fig. 6 was approximately 47 °C. This can be explained by the position of the thermocouple, which was attached to the sample surface. The surface temperature was lower than the internal temperature; thus, there were small differences in the phase-change temperature. As shown in Fig. 6, sample P0, with no PCM, maintained a consistent cooling speed between 50 and 45 °C. In contrast, the cooling speed of the samples containing PCM decreased in this range, as the PCM changed phase. This was deduced from the phase change process of the PCM. Heat energy is released as the PCM changes from liquid to solid, indicating latent heat energy release [35]. Therefore, the samples with PCM showed greater heat storage capability during the cooling test, and this phenomenon increased as the PCM content increased. Specifically, it should be noted that the heat storage performance obtained from the PCM phase change was maintained, even when the number of cooling cycles increase, demonstrating the high durability of the PCM, as shown in Fig. 6.

The slope of the temperature decrease observed at temperatures of 50–45 °C was calculated and is shown in Fig. 7. All the samples, regardless of their PCM content, showed a relatively stable cooling speed during the cyclic cooling test. Sample P0 had a cooling speed of 0.0175 °C/s in the first cycle, which was faster than samples P5, P10, P20, and P30, having cooling speeds of 0.0143, 0.0141, 0.0128, and 0.0126 °C/s, respectively. The cooling speed decreased as the PCM content increased because the latent heat energy was proportional to the PCM content. The cooling speeds of samples P0, P5, P10, P20, and P30 changed to 0.0189, 0.0139, 0.0114, 0.0106, and 0.0106 °C/s, respectively, by the 20th cycle, indicating the stability of the heat storage performance. According to the cooling speed results in Fig. 7, the incorporation of PCM enhanced the heat storage performance of the cement-based self-heating composites, which can improve their energy efficiency. In addition, it can be found that the incorporation of 20 wt% of PCM is optimized content to ensure the improved heat storage capability considering the volume and conductive fillers contents of the samples used in this study.

The self-heating and heat storage performances were investigated simultaneously during five cyclic heating–cooling tests, as shown in Fig. 8 and Fig. S1. Here, heating and cooling times of 3 h and 2 h, respectively, were selected to observe temperature saturation. After each heating cycle, the samples exhibited a surface temperature of approximately 55 °C because the same input power (i.e., 10 W) was applied to the samples. At temperatures of 40–45 °C, the PCM phase

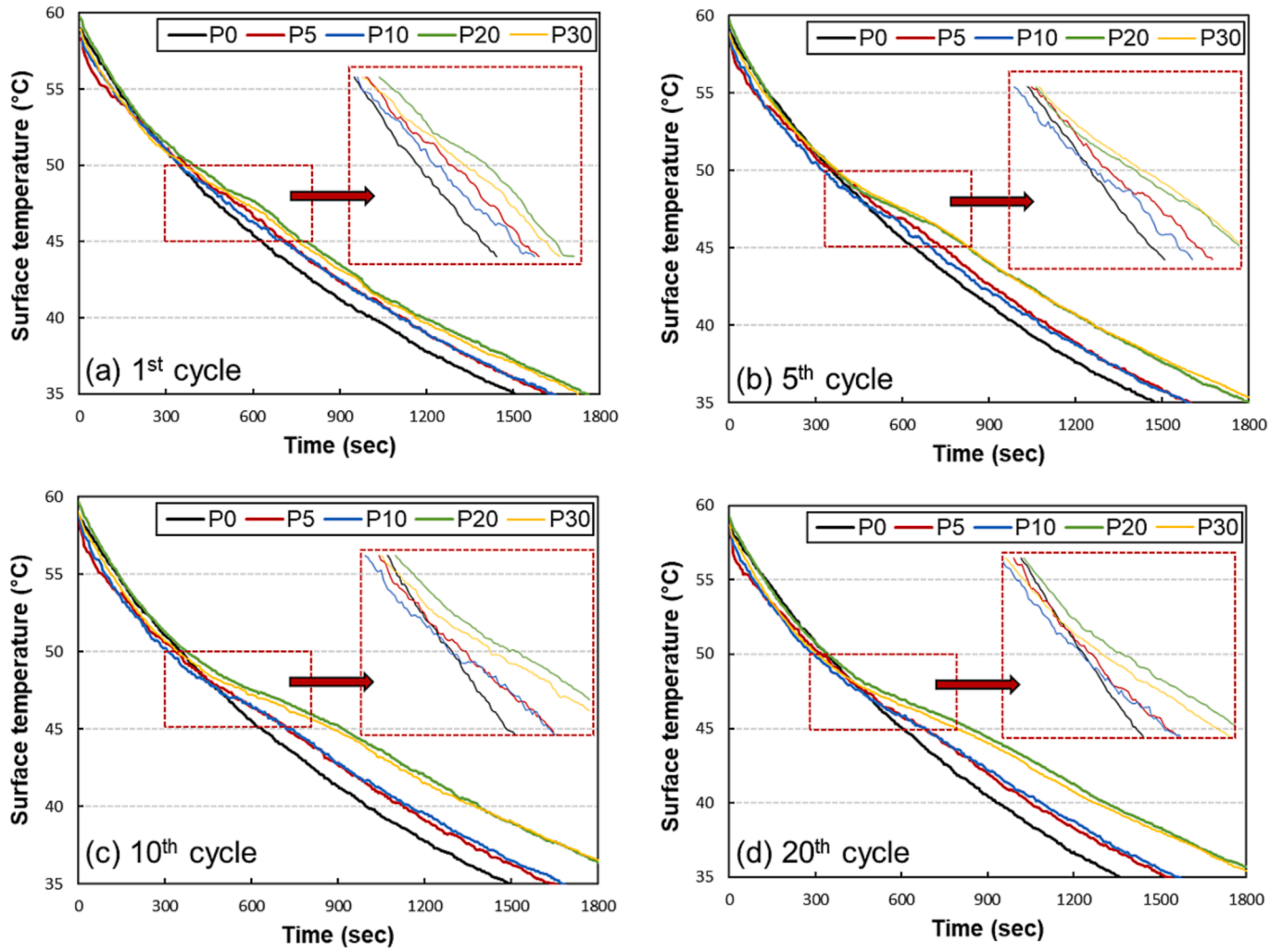

Fig. 6. Variations in the surface temperature of the samples observed in the cyclic cooling test with (a) 1st, (b) 5th, (c) 10th, and (d) 20th cycles.

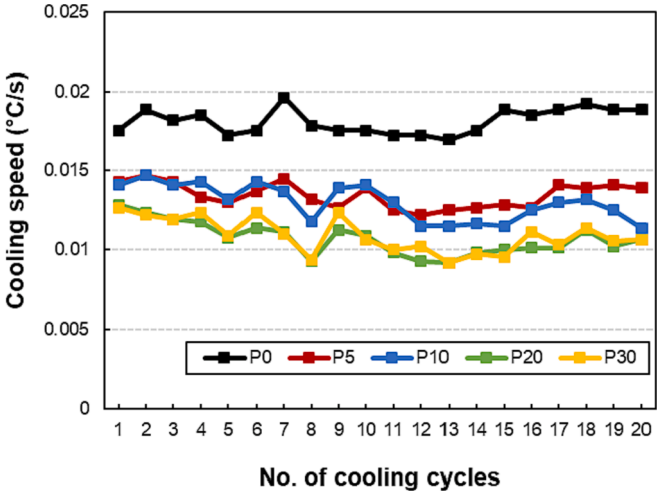

Fig. 7. Cooling speed of the samples as the temperature decreased from 50 to 45 °C observed in the cyclic cooling test.

change was observed during the heating and cooling cycles. Specifically, the samples containing PCM cooled more slowly than the sample without PCM (i.e., P0), which increased their heat storage performance. However, it should be noted that the voltage required to obtain the same input power (i.e., 10 W) increased as the number of cycles increased, as shown in Fig. 8. For the first cycle, input voltages of 5.5, 5.3, 6.5, 8.3, and 14.4 V were required to apply 10 W to samples P0, P5, P10, P20, and P30, respectively. By the 5th cycle, these values had increased to 5.8, 5.3, 6.6, 9.0, and 17.8 V, respectively; an increase of approximately 24 % for sample P30. An increase in the required input voltage can expose the cementitious composites to thermal shock, reducing their heating performance [33].

Although sample P30 showed temperature increases similar to or higher than the other samples during heating, the required input voltage increased significantly as the number of cycles increased. This phenomenon can be inferred from the disconnection of conductive pathways during cyclic heating. This is because the PCM particles can reduce connectivity of the conductive networks when the conductive fillers expand as the temperature increases, as shown by the electrical resistivity stability results in Fig. 5e. Consequently, it can be said that an appropriate PCM content can improve the self-heating capability in terms of heating efficiency, but excessive PCM content can reduce the heating performance owing to an increase in electrical resistivity.

5. Effects of PCM addition on cyclic heating and heat-storage capacities of the samples

Based on the experimental results, it is found that the addition of PCM can improve the heat-storage capacity of cement-based self-heating composites; however, it was found that the excessive amount of PCM

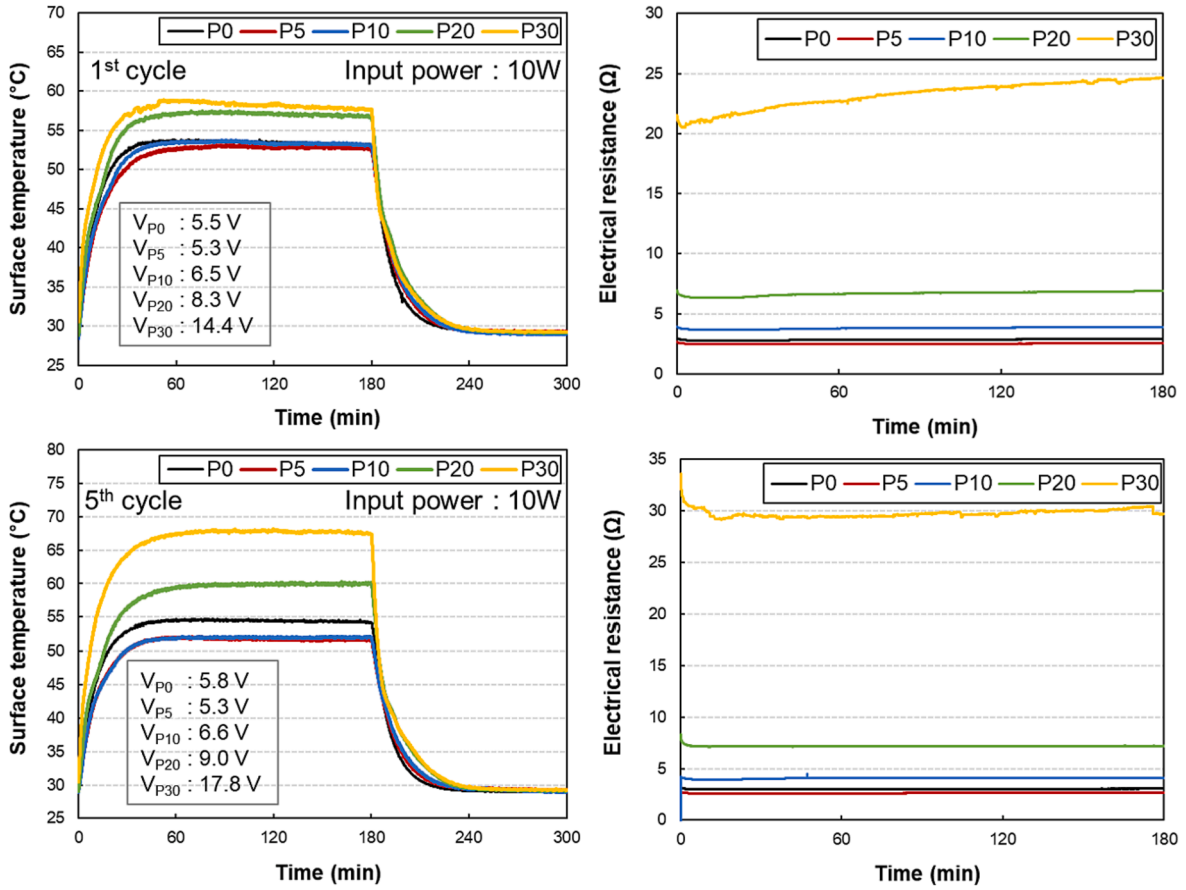

Fig. 8. Variations in the surface temperature and electrical resistance of the samples at 1st and 5th cycles.

may degrade their self-heating performance even the heat-storage capacity is improved. The heat-storage capacity is related to the phase change mechanisms of PCM; thus, the microstructural analysis was conducted to deeply analyze the effects of PCM inclusion on changes of self-heating performance and heat-storage capacity. In Fig. 9, the DSC heat flow measurements for the samples during the exothermic and endothermic processes are shown. There were two main peaks in both graphs. The main transition peak occurred at a higher temperature and corresponded to a solid-to-liquid phase change of the PCM. The minor transition peak occurred at a lower temperature and corresponded to a solid-to-solid phase change [34,35].

shows that the melting temperature of the PCM was approximately 58–59 °C, whereas a solid-to-solid phase change occurred at 56 °C in the exothermic process. These observed temperatures support the presence of phase change zones observed in the self-heating and cooling tests, as shown in Fig. 8. Based on the DSC heat flow results, the latent heat values were calculated using the total area under the two main transition peaks where solid-to-solid and solid-to-liquid transitions occurred (Fig. 9), as summarized in Table 3. Samples P0, P5, P10, P20, and P30 showed latent heat energy of 0, 1.58, 3.16, 6.40, and 8.29 J/g and 0, 1.40, 3.47, 7.41, and 10.95 J/g during the exothermic and endothermic processes, respectively, with the increase in PCM contents from 0 to 30 %. Thus, the latent heat increased as the PCM content increased, showing increases in latent heat of approximately 424 % and 682 % in exothermic and endothermic processes, respectively. Considering the PCM content, these latent heats are similar to or greater than those found in previous studies [34,35]. Consequently, the DSC heat flow results revealed that the PCM can increase the latent heat energy, which is sufficient to improve the heat storage performance of conductive cementitious heating composites. However, as seen in self-heating experiments results, it should be noted that the excessive amount of PCM

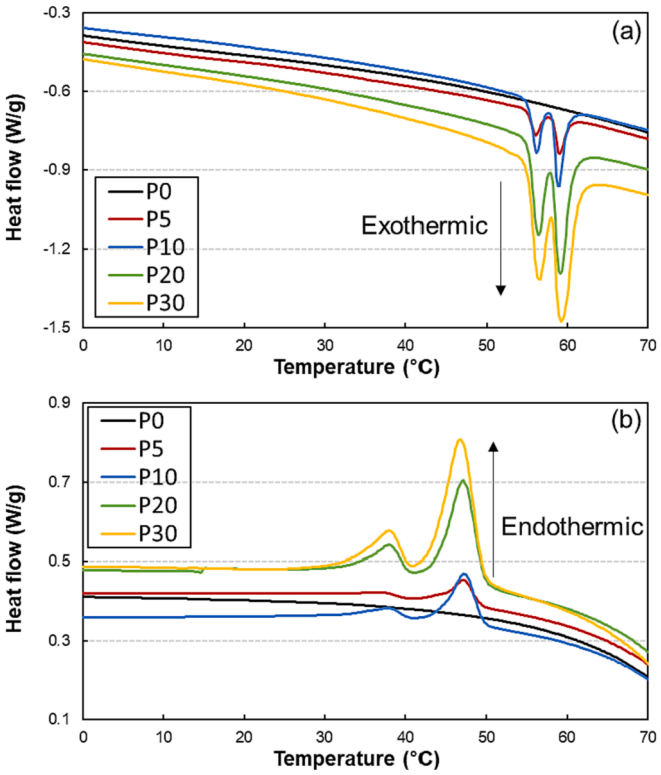

Fig. 9. Heat flow in the samples observed during (a) exothermic and (b) endothermic processes.

Table 3
Latent heat energy of the samples observed during the exothermic and endothermic processes.

Sample	Latent heat energy (J/g)				
	P0	P5	P10	P20	P30
Exothermic	0.00	1.58	3.16	6.40	8.29
Endothermic	0.00	1.40	3.47	7.41	10.95

(i.e., 30 % by cement mass) can degrade the self-heating performance. The requirement of high latent heat energy to increase the temperature of this composite resulted in lower temperature increase, thus a lower PCM content (~20 %) should be used.

Meanwhile, the micro-CT was used for 3D tomography analysis of samples in order to assess the dispersion of PCM and calculated the percent PCM content (as shown in Fig. 10). Cross-sectional images of the samples were obtained, and the images were labeled with the PCM content. Based on these images, the 3D tomography results were obtained, as shown in Fig. 10 (a). These results showed that the PCM was well dispersed in the cementitious composites, even as the embedded PCM content increased from 0 to 30 %. In addition, the PCM content can be calculated using micro-CT, as shown in Fig. 10 (b). The particle size and density can be set in micro-CT observation; thus, it is possible to compare the volume percentage of the embedded PCM by comparing with the reference P0 sample without incorporating PCM [55]. The results showed that the PCM contents of P10, P20, and P30 were 11.7, 22.4, and 27.4 vol%, respectively as seen in Fig. 10. The results obtained from these analyses are in close agreements with the cyclic heating and heat-storage test results. These findings have not been actively reported in the previous related studies; thus, these findings can be a step towards developments of cement-based self-heating systems.

6. Concluding remarks

In this study, the effects of PCM addition on the self-heating performance and heat-storage capacity of cementitious self-heating composites were investigated. Five PCM contents (0, 5, 10, 20, and 30 wt%) were considered, and their effects on the characterization, heat-generation, and heat-storage performances were investigated systematically. The test results were analyzed using DSC and micro-CT observations. The main conclusions can be summarized as follows:

(1) The addition of the PCM increased the electrical resistivity and decreased the thermal and compressive strengths. In particular, the addition of 30 wt% of PCM increased the electrical resistivity dramatically, and a high input voltage was required to obtain a favorable heat-generation capability.
(2) The electrical resistivity of the sample with 30 wt% of PCM increased by approximately 350 % during the cyclic heating test, which lowered the heat generation stability from 30 to 6 °C. Thus, it can be said that an excessive amount of PCM may negatively affect the heating performance.
(3) Cooling speeds of the samples with 0, 5, 10, 20, and 30 wt% of PCM were recorded. It can be found that the addition of PCM reduced the cooling speed and improved the heat storage capacity.
(4) The DSC test results indicated that the samples with 0, 5, 10, 20, and 30 wt% of PCM had latent heat energies of 0, 1.40, 3.47, 7.41, and 10.95 J/g, respectively, during the endothermic process. This showed that improvements in the latent heat energy can enhance the heat storage performance.

The experimental results in this study can contribute to investigating the effects of PCM addition on the self-heating performance and heat-storage capacity of cementitious self-heating composites. However, the evaluation on durability of the PCM-incorporated cementitious composites has not been conducted. Therefore, based on the present experimental results, the further studies will be carried out to investigate the durability of the fabricated composites as exposed to various weathering conditions (e.g., Carbonation, water ingress, and freeze–thaw cycles). In addition, the mock-up test using the fabricated composites with optimized mix-proportions will be conducted.

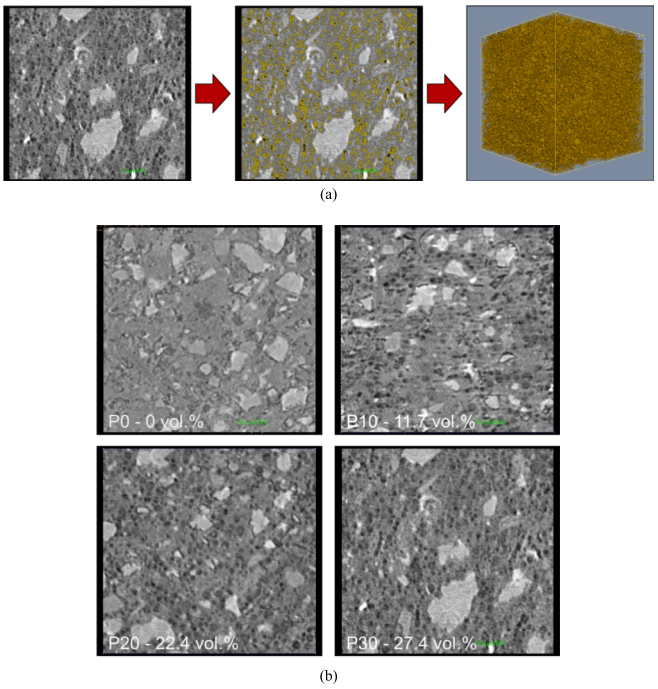

Fig. 10. Internal structural analysis results of the samples containing PCM via micro-CT: (a) 3D visualization of PCM distribution and (b) calculated volume percentage of PCM.

CRediT authorship contribution statement

Daeik Jang: Conceptualization, Methodology, Investigation, Validation, Data curation, Formal analysis, Writing – original draft. **H.N. Yoon:** Validation, Data curation, Writing – review & editing. **Beomjoo Yang:** Resources, Writing – review & editing, Funding acquisition. **Hammad R. Khalid:** Methodology, Validation, Resources, Writing – review & editing, Supervision.

Declaration of Competing Interest

The authors declare that they have no known competing financial interests or personal relationships that could have appeared to influence the work reported in this paper.

Data availability

Data will be made available on request.

Acknowledgment

This work was supported by the National Research Foundation of Korea grant funded by the Korean government (MSIT) (2020R1C1C1005063). The support of King Fahd University of Petroleum & Minerals, Dhahran, Saudi Arabia, is also acknowledged.

Appendix A. Supplementary data

Supplementary data to this article can be found online at https://doi.

org/10.1016/j.conbuildmat.2023.130512.

References

[1] W. Dong, W. Li, X. Zhu, D. Sheng, S.P. Shah, Multifunctional cementitious composites with integrated self-sensing and hydrophobic capacities toward smart structural health monitoring, Cem. Concr. Compos. 118 (2021), 103962, https://doi.org/10.1016/j.cemconcomp.2021.103962.

[2] D. Jang, H.N. Yoon, B. Yang, J. Seo, S.Z. Farooq, H.K. Lee, Synergistic effects of CNT and CB inclusion on the piezoresistive sensing behaviors of cementitious composites blended with fly ash, Smart Struct. Syst. 2 (2022) 351–359.

[3] S.-J. Lee, I. You, S. Kim, H.-O. Shin, D.-Y. Yoo, Self-sensing capacity of ultra-high-performance fiber-reinforced concrete containing conductive powders in tension, Cem. Concr. Compos. 125 (2021), 104331, https://doi.org/10.1016/j.cemconcomp.2021.104331.

[4] Z. Tian, Y. Li, J. Zheng, S. Wang, A state-of-the-art on self-sensing concrete: Materials, fabrication and properties, Compos. Part B Eng. 177 (2019), 107437, https://doi.org/10.1016/j.compositesb.2019.107437.

[5] D. Jang, J. Bang, H.N. Yoon, J. Seo, J. Jung, Deep learning - based LSTM model for prediction of long - term piezoresistive sensing performance of cement - based sensors incorporating multi - walled carbon nanotube, Comput. Concr. 30 (2022) 301–310. https://doi.org/10.12989/cac.2022.30.5.301.

[6] L. Zhang, L. Li, Y. Wang, X. Yu, B. Han, Multifunctional cement-based materials modified with electrostatic self-assembled CNT/TiO2 composite filler, Constr. Build. Mater. 238 (2020), 117787, https://doi.org/10.1016/j.conbuildmat.2019.117787.

[7] Z. Liu, H. Ge, J. Wu, J. Chen, Enhanced electromagnetic interference shielding of carbon fiber/cement composites by adding ferroferric oxide nanoparticles, Constr. Build. Mater. 151 (2017) 575–581, https://doi.org/10.1016/j.conbuildmat.2017.06.017.

[8] D. Jang, B.H. Choi, H.N. Yoon, B. Yang, H.K. Lee, Improved electromagnetic wave shielding capability of carbonyl iron powder-embedded lightweight CFRP composites, Compos. Struct. 286 (2022), 115326, https://doi.org/10.1016/j.compstruct.2022.115326.

[9] X. Wang, Q. Li, H. Lai, Y. Peng, S. Xu, Broadband microwave absorption enabled by a novel carbon nanotube gratings/cement composite metastructure, Compos. Part B Eng. 242 (2022), 110071, https://doi.org/10.1016/j.compositesb.2022.110071.

[10] J. Gomis, O. Galao, V. Gomis, E. Zornoza, P. Garcés, Self-heating and deicing conductive cement. Experimental study and modeling, Constr. Build. Mater. 75 (2015) 442–449, https://doi.org/10.1016/j.conbuildmat.2014.11.042.

[11] D. Jang, H.N. Yoon, J. Seo, S. Park, Enhanced electrical heating capability of CNT-embedded cementitious composites exposed to water ingress with addition of silica aerogel, Ceram. Int. 48 (2022) 13356–13365, https://doi.org/10.1016/j.ceramint.2022.01.216.

[12] M. Hambach, H. Möller, T. Neumann, D. Volkmer, Carbon fibre reinforced cement-based composites as smart floor heating materials, Compos. Part B Eng. 90 (2016) 465–470, https://doi.org/10.1016/j.compositesb.2016.01.043.

[13] W. Tian, Y. Liu, W. Wang, Enhanced ohmic heating and chloride adsorption efficiency of conductive seawater cementitious composite: Effect of non-conductive nano-silica, Compos. Part B Eng. 236 (2022), 109854, https://doi.org/10.1016/j.compositesb.2022.109854.

[14] A.O. Monteiro, P.B. Cachim, P.M.F.J. Costa, Self-sensing piezoresistive cement composite loaded with carbon black particles, Cem. Concr. Compos. 81 (2017) 59–65, https://doi.org/10.1016/j.cemconcomp.2017.04.009.

[15] W.-L. Yao, G. Xiong, Y. Yang, H.-Q. Huang, Y.-F. Zhou, Effect of silica fume and colloidal graphite additions on the EMI shielding effectiveness of nickel fiber cement based composites, Constr. Build. Mater. 150 (2017) 825–832.

[16] E. Teomete, The effect of temperature and moisture on electrical resistance, strain sensitivity and crack sensitivity of steel fiber reinforced smart cement composite, Smart Mater. Struct. 25 (7) (2016) 075024.

[17] M.K. Hassanzadeh-Aghdam, M.J. Mahmoodi, M. Safi, Effect of adding carbon nanotubes on the thermal conductivity of steel fiber-reinforced concrete, Compos. Part B Eng. 174 (2019), 106972, https://doi.org/10.1016/j.compositesb.2019.106972.

[18] M.S.D.C. Dela Vega, M.R. Vasquez, Plasma-functionalized exfoliated multilayered graphene as cement reinforcement, Compos. Part B Eng. 160 (2019) 573–585, https://doi.org/10.1016/j.compositesb.2018.12.055.

[19] H.M. Park, S.M. Park, S.M. Lee, I.J. Shon, H. Jeon, B.J. Yang, Automated generation of carbon nanotube morphology in cement composite via data-driven approaches, Compos. Part B Eng. 167 (2019) 51–62, https://doi.org/10.1016/j.compositesb.2018.12.011.

[20] D. Jang, H.N. Yoon, S.Z. Farooq, H.K. Lee, I.W. Nam, Influence of water ingress on the electrical properties and electromechanical sensing capabilities of CNT / cement composites, J. Build. Eng. 42 (2021), 103065, https://doi.org/10.1016/j.jobe.2021.103065.

[21] Y. Gao, H.W. Jing, S.J. Chen, M.R. Du, W.Q. Chen, W.H. Duan, Influence of ultrasonication on the dispersion and enhancing effect of graphene oxide–carbon nanotube hybrid nanoreinforcement in cementitious composite, Compos. Part B Eng. 164 (2019) 45–53, https://doi.org/10.1016/j.compositesb.2018.11.066.

[22] O. Öztürk, G. Yıldırım, Ü.S. Keskin, H. Siad, M. Şahmaran, Nano-tailored multi-functional cementitious composites, Compos. Part B Eng. 182 (2020) 107670.

[23] G.M. Kim, B.J. Yang, H.N. Yoon, H.K. Lee, Synergistic effects of carbon nanotube and carbon fiber on heat generation and electrical characteristics of cementitious composites, Carbon N. Y. 134 (2018) 283–292, https://doi.org/10.1016/j.carbon.2018.03.070.

[24] H.N. Yoon, D. Jang, H.K. Lee, I.W. Nam, Influence of carbon fiber additions on the electromagnetic wave shielding characteristics of CNT-cement composites, Constr. Build. Mater. 269 (2021) 121238.

[25] G.M. Kim, F. Naeem, H.K. Kim, H.K. Lee, Heating and heat-dependent mechanical characteristics of CNT-embedded cementitious composites, Compos. Struct. 136 (2016) 162–170, https://doi.org/10.1016/j.compstruct.2015.10.010.

[26] H. Lee, S. Jeong, S. Park, W. Chung, Enhanced mechanical and heating performance of multi-walled carbon nanotube-cement composites fabricated using different mixing methods, Compos. Struct. 225 (2019), 111072, https://doi.org/10.1016/j.compstruct.2019.111072.

[27] A. Arabzadeh, H. Ceylan, S. Kim, A. Sassani, K. Gopalakrishnan, M. Mina, Electrically-conductive asphalt mastic: Temperature dependence and heating efficiency, Mater. Des. 157 (2018) 303–313, https://doi.org/10.1016/j.matdes.2018.07.059.

[28] Z. Tang, D. Lu, J. Gong, X. Shi, Self-Heating Graphene Nanocomposite Bricks : A Case Study in China, Materials (Basel). 13 (2020) 1–13, https://doi.org/10.3390/ma13030714.

[29] X. Wang, Y. Wu, P. Zhu, T. Ning, Snow Melting Performance of Graphene Composite Conductive Concrete in Severe Cold Environment, Materials (Basel). 14 (21) (2021) 6715.

[30] D. Jang, H.N. Yoon, J. Seo, S. Park, T. Kil, H.K. Lee, Improved electric heating characteristics of CNT-embedded polymeric composites with an addition of silica aerogel, Compos. Sci. Technol. 212 (2021), 108866, https://doi.org/10.1016/j.compscitech.2021.108866.

[31] Y. Liu, M. Wang, W. Wang, Ohmic heating curing of electrically conductive carbon nanofiber/cement-based composites to avoid frost damage under severely low temperature, Compos. Part A Appl. Sci. Manuf. 115 (2018) 236–246, https://doi.org/10.1016/j.compositesa.2018.10.008.

[32] Y.C. Choi, Cyclic heating and mechanical properties of CNT reinforced cement composite, Compos. Struct. 256 (2021), 113104, https://doi.org/10.1016/j.compstruct.2020.113104.

[33] D. Jang, H.N. Yoon, J. Seo, H.K. Lee, G.M. Kim, Effects of silica aerogel inclusion on the stability of heat generation and heat-dependent electrical characteristics of cementitious composites with CNT, Cem. Concr. Compos. 115 (2021), 103861, https://doi.org/10.1016/j.cemconcomp.2020.103861.

[34] M. Frąc, W. Pichór, P. Szołdra, W. Szudek, Cement composites with expanded graphite/paraffin as storage heater, Constr. Build. Mater. 275 (2021), https://doi.org/10.1016/j.conbuildmat.2020.122126.

[35] Y.U. Kim, J.H. Park, B.Y. Yun, S. Yang, S. Wi, S. Kim, Mechanical and thermal properties of artificial stone finishing materials mixed with PCM impregnated lightweight aggregate and carbon material, Constr. Build. Mater. 272 (2021), 121882, https://doi.org/10.1016/j.conbuildmat.2020.121882.

[36] M. Tafesse, N. Kon, A. Shiferaw, H. Kyoung, S. Wook, H. Kim, Flowability and electrical properties of cement composites with mechanical dispersion of carbon nanotube, Constr. Build. Mater. 293 (2021), 123436, https://doi.org/10.1016/j.conbuildmat.2021.123436.

[37] M.J. Lim, H.K. Lee, I.W. Nam, H.K. Kim, Carbon nanotube/cement composites for crack monitoring of concrete structures, Compos. Struct. 180 (2017) 741–750, https://doi.org/10.1016/j.compstruct.2017.08.042.

[38] H.K. Lee, I.W. Nam, M. Tafesse, H.K. Kim, Fluctuation of electrical properties of carbon-based nanomaterials/cement composites: Case studies and parametric modeling, Cem. Concr. Compos. 102 (2019) 55–70, https://doi.org/10.1016/j.cemconcomp.2019.04.008.

[39] D. Jang, H.N. Yoon, J. Seo, H.J. Cho, G.M. Kim, Y.-K. Kim, B. Yang, Improved electromagnetic interference shielding performances of carbon nanotube and carbonyl iron powder (CNT@CIP)-embedded polymeric composites, J. Mater. Res. Technol. 18 (2022) 1256–1266, https://doi.org/10.1016/j.jmrt.2022.02.134.

[40] H.K. Kim, I.W. Nam, H.K. Lee, Enhanced effect of carbon nanotube on mechanical and electrical properties of cement composites by incorporation of silica fume, Compos. Struct. 107 (2014) 60–69, https://doi.org/10.1016/j.compstruct.2013.07.042.

[41] J. Seo, S.J. Bae, D.I. Jang, S. Park, B. Yang, H.K. Lee, Thermal behavior of alkali-activated fly ash/slag with the addition of an aerogel as an aggregate replacement, Cem. Concr. Compos. 106 (2020), 103462, https://doi.org/10.1016/j.cemconcomp.2019.103462.

[42] J. Seo, S. Kim, D. Jang, H. Kim, H.K. Lee, Internal carbonation of belite-rich Portland cement: An in-depth observation at the interaction of the belite phase with sodium bicarbonate, J. Build. Eng. 44 (2021), 102907, https://doi.org/10.1016/j.jobe.2021.102907.

[43] M. Bhandari, J. Wang, D. Jang, IlWoo Nam, B. Huang, A Comparative Study on the Electrical and Piezoresistive Sensing Characteristics of GFRP and CFRP Composites with Hybridized Incorporation of Carbon Nanotubes, Graphenes, Carbon Nanofibers, and Graphite Nanoplatelets, Sensors 21 (21) (2021) 7291.

[44] G.M. Kim, S.M. Park, G.U. Ryu, H.K. Lee, Electrical characteristics of hierarchical conductive pathways in cementitious composites incorporating CNT and carbon fiber, Cem. Concr. Compos. 82 (2017) 165–175, https://doi.org/10.1016/j.cemconcomp.2017.06.004.

[45] I. Asadi, P. Shafigh, Z.F.B. Abu Hassan, N.B. Mahyuddin, Thermal conductivity of concrete – A review, J. Build. Eng. 20 (2018) 81–93.

[46] S.Y. Kim, H.G. Jang, C.M. Yang, B.J. Yang, Multiscale prediction of thermal conductivity for nanocomposites containing crumpled carbon nanofillers with interfacial characteristics, Compos. Sci. Technol. 155 (2018) 169–176, https://doi.org/10.1016/j.compscitech.2017.12.011.

[47] J. Yang, H. Wu, G. Huang, Y. Liang, Y. Liao, Modeling and coupling effect evaluation of thermal conductivity of ternary opacifier/fiber/aerogel composites

for super-thermal insulation, Mater. Des. 133 (2017) 224–236, https://doi.org/10.1016/j.matdes.2017.07.056.
[48] J. Rostami, O. Khandel, R. Sedighardekani, A.R. Sahneh, S.A. Ghahari, Enhanced workability, durability, and thermal properties of cement-based composites with aerogel and paraffin coated recycled aggregates, J. Clean. Prod. 297 (2021), 126518, https://doi.org/10.1016/j.jclepro.2021.126518.
[49] D. Jang, T. Kil, H.N. Yoon, J. Seo, H.R. Khalid, Artificial neural network approach for predicting tunneling-induced and frequency-dependent electrical impedances of conductive polymeric composites, Mater. Lett. 302 (2021), 130420, https://doi.org/10.1016/j.matlet.2021.130420.
[50] J.-E. Park, G.-E. Yun, D.-I. Jang, Y.-K. Kim, Analysis of electrical resistance and impedance change of magnetorheological gels with DC and AC voltage for magnetometer application, Sensors (Switzerland). 19 (11) (2019) 2510.
[51] N. Hu, Y. Karube, C. Yan, Z. Masuda, H. Fukunaga, Tunneling effect in a polymer/carbon nanotube nanocomposite strain sensor, Acta Mater. 56 (2008) 2929–2936, https://doi.org/10.1016/j.actamat.2008.02.030.
[52] D. Jang, H.N. Yoon, J. Seo, B. Yang, Effects of exposure temperature on the piezoresistive sensing performances of MWCNT-embedded cementitious sensor, J. Build. Eng. 47 (2022), 103816, https://doi.org/10.1016/j.jobe.2021.103816.
[53] G.M. Kim, I.W. Nam, B. Yang, H.N. Yoon, H.K. Lee, S. Park, Carbon nanotube (CNT) incorporated cementitious composites for functional construction materials: The state of the art, Compos. Struct. 227 (2019), 111244, https://doi.org/10.1016/j.compstruct.2019.111244.
[54] H. Shifeng, X. Dongyu, C. Jun, X. Ronghua, L. Lingchao, C. Xin, Smart properties of carbon fiber reinforced cement-based composites, J. Compos. Mater. 41 (2007) 125–131, https://doi.org/10.1177/0021998306063378.
[55] H. Min Park, S. Park, I.J. Shon, G.M. Kim, S. Hwang, M. Wook Lee, B. Yang, Influence of Portland cement and alkali-activated slag binder on the thermoelectric properties of the p-type composites with MWCNT, Constr. Build. Mater. 292 (2021), 123393, https://doi.org/10.1016/j.conbuildmat.2021.123393.